

APPLIED SCIENCES AND ENGINEERING

Self-contained soft electrofluidic actuators

Wei Tang¹, Yangqiao Lin¹, Chao Zhang^{1*}, Yuwen Liang¹, Jinrong Wang¹, Wei Wang¹, Chen Ji², Maoying Zhou³, Huayong Yang¹, Jun Zou^{1,4*}

Soft robotics revolutionized human-robot interactions, yet there exist persistent challenges for developing high-performance soft actuators that are powerful, rapid, controllable, safe, and portable. Here, we introduce a class of self-contained soft electrofluidic actuators (SEFAs), which can directly convert electrical energy into the mechanical energy of the actuators through electrically responsive fluids that drive the outside elastomer deformation. The use of special dielectric liquid enhances fluid flow capabilities, improving the actuation performance of the SEFAs. SEFAs are easily manufactured by using widely available materials and common fabrication techniques, and display excellent comprehensive performances in portability, controllability, rapid response, versatility, safety, and actuation. An artificial muscle stretching a joint and a soft bionic ray swimming in a tank demonstrate their effective performance. Hence, SEFAs offer a platform for developing soft actuators with potential applications in wearable assistant devices and soft robots.

INTRODUCTION

In contrast to conventional rigid robots, soft robots (1–8) made from flexible materials offer great advantages in adapting to complex surroundings, performing autonomous tasks, and mimicking the motions and functions of biological systems, which have the potential to be used for more compliant and safer devices that operate close to or even in human. A lot of impressive and attractive work about soft robots have been reported. For example, Shepherd *et al.* (4) introduced a pneumatically actuated quadrupedal robot that could move in narrow spaces. Mao *et al.* (5) fabricated a flower-shaped robot with five soft electromagnetic actuator petals, of which each petal can be programmed and operate very fast. Tang *et al.* (6) developed a high-speed cheetah-like galloping crawlers with ultra-fast locomotion speeds of 2.68 body length per second by skillfully leveraging elastic instabilities for improving performances of soft pneumatic robots.

As the core component of soft robots, there exist persistent challenges for developing high-performance soft actuators that can achieve several indispensable properties, including controllability, portability, durability, safety, versatility, rapid response, and excellent actuation. Different from rigid actuators, soft actuators (5, 9–16) need to deform themselves to achieve the motions or operations of soft robots. On the basis of different actuation and deformation mechanisms, a wide variety of soft actuators have been reported. Among these, traditional soft fluidic (pneumatic or hydraulic) actuators (6, 15) are most prevalent because of their simple and versatile designs. Nevertheless, the requirement of external bulky, rigid compressors or pumps for supplying for pressurized fluids limits their portability (17–19). Besides, many portable soft actuators (9–10, 13–14) driven by external stimulus, such as thermal energy, magnetism, humidity, and light, have also been developed. Although they have some own particular merits in some areas, some remarkable shortcomings, such as poor controllability and slow response speed, prohibit their widespread applications. For example, shape

memory alloy actuators can provide large actuation force and high-power density (20), but the lack of controllability limits their applications because of poor control of thermal energy (21). Compared with other stimuli-responsive soft actuators, the development of advanced electrically responsive soft actuators has attracted considerable interests because the electricity, as the most commonly used energy, has excellent controllability and is easily compatible or seamlessly integrated with existing electric-driven products in our life and industry, providing the best platform for popularizing these soft actuators. Dielectric elastomer (DE) actuators (22–24) can achieve actuation of elastomer films through electrostatic extrusion effect between equal-area positive and negative electrode pairs, which stand out among various electrically responsive actuators for their rapid and controllable actuation with large amplitudes. Nevertheless, the dielectric breakdown seems to be a challenge for their reliable applications (25–26). Recently, a class of HASEL (hydraulically amplified self-healing electrostatic) actuators (11) were developed by replacing the solid dielectric inside the DE actuators with liquid dielectric, allowing for self-healing after dielectric breakdown. In addition to electrostatic extrusion mechanism, electroconjugate fluid (ECF) is a kind of electrically responsive functional fluid that can produce strong jet under a nonuniform electric field. The ECF jet pumps have been used to power soft robotic hands (27), inchworms (28), and muscle cells (29). The ECF jetting method provides a good way to address the poor portability problem of traditional soft fluidic actuators, while retaining the advantages of their simple and versatile designs. Current applications of ECF to soft actuators mainly focus on fluidic actuators driven by the separated ECF pumps, limiting the response speed of fluidic actuators. The more compact and simpler architecture of soft fluidic actuators that highly integrate ECF pumps, tubes, liquid reservoirs, and actuators still needs to be explored to further improve the response speeds of fluidic actuators.

Here, we introduce a class of self-contained soft electrofluidic actuators (SEFAs), which mainly use electrically responsive fluids to drive the external elastomer pouch deformation. SEFAs have a simple and compact architecture with a rod positive electrode immersed in dielectric liquid and the ground electrodes coating the pouch surface, thereby guaranteeing that the actuators can be fully enclosed in a closed electrode region to generate ECF jet of dielectric liquid. Meanwhile, a method of dissociating hydrogel into dielectric

Copyright © 2021
The Authors, some
rights reserved;
exclusive licensee
American Association
for the Advancement
of Science. No claim to
original U.S. Government
Works. Distributed
under a Creative
Commons Attribution
NonCommercial
License 4.0 (CC BY-NC).

¹State Key Laboratory of Fluid Power and Mechatronic Systems, Zhejiang University, Hangzhou 310027, China. ²Institute of Marine Science and Technology, Shandong University, Qingdao 266237, China. ³School of Mechanical Engineering, Hangzhou Dianzi University, Hangzhou 310027, China. ⁴Ningbo Research Institute, Zhejiang University, Ningbo 315100, China.

*Corresponding author. Email: chao.zhang@zju.edu.cn (C.Z.); junzou@zju.edu.cn (J.Z.)

liquid is proposed to further enhance the ECF effect, improving the actuation performances of SEFAs. SEFAs have several distinctive qualities: (i) SEFAs that highly integrate pumps, tubes, liquid reservoirs, and actuators not only exhibit good portability but also achieve excellent response to electrical signals; (ii) SEFAs have good safety because the high-voltage positive electrodes are encapsulated in dielectric liquid and the positive electrodes also do not need to deform during the actuation process; (iii) SEFAs are versatile, which can easily achieve different actuation modes, such as linear actuation and bending actuation, by just adjusting the stiffness or thickness of the external membrane shell; (iv) SEFAs have high environment adaptability, which enables them to operate in both water and air; (v) SEFAs are electrically powered, which grants them good compatibility with existing electric-driven products; (vi) SEFAs can be easily manufactured using basic fabrication techniques and widely available materials; thus, it is easy to be popularized. Successful applications of SEFAs in an artificial muscle stretching a joint and a soft bionic ray swimming in a tank demonstrate their excellent performances, illustrating their great potential to be popularized in soft robotics.

RESULTS

We design a linear SEFA that consists of a flexible pouch, dielectric liquid, and a rod positive electrode (Fig. 1A, figs. S1 and S2, and movie S1). SEFAs have high adaptability, which can operate in both

water and air: When the rod electrode acts as a high-voltage positive electrode, the water can serve as the electric ground according to the work of Li *et al.* (30), while the carbon grease should be coated on the actuator surface as grounding electrodes in air. As shown in movie S2, the dielectric liquids are ECF liquids that can produce the typical ECF jet phenomenon when a DC high voltage is applied. Figure 1B illustrates the schematic of actuation mechanism. SEFA is made of a rod positive electrode and spindle grounding electrodes. When the voltage is applied, a nonuniform electric field is generated throughout the dielectric liquid between electrodes with very different shapes. In such nonuniform and strong electric field, Wien effect occurs. The Wien effect (31–37) is a phenomenon in which the equilibrium between ion pairs and free ions is destroyed and the dissociation rate becomes greater than the recombination rate when the dielectric liquid is under the strong nonuniform electric field. This is because uncontrolled chemical impurities exist naturally in even a pure dielectric liquid. In the bulk, the rate of ion dissociation is basically in equilibrium with that of ion recombination so that it is almost neutralized throughout the dielectric liquid. However, local variation of the field intensity leads to a nonzero gradient of the ion concentrations, which then causes a relatively small amount of concentration difference between the cation and anion, corresponding to nonuniform field-induced space charge density. The space charge density can be given by the formula $q = -KE \cdot \nabla E$ (31–33, 35, 37–38), where $K = 2\epsilon_0\epsilon_r\gamma > 0$ is a constant (ϵ_0 and ϵ_r are

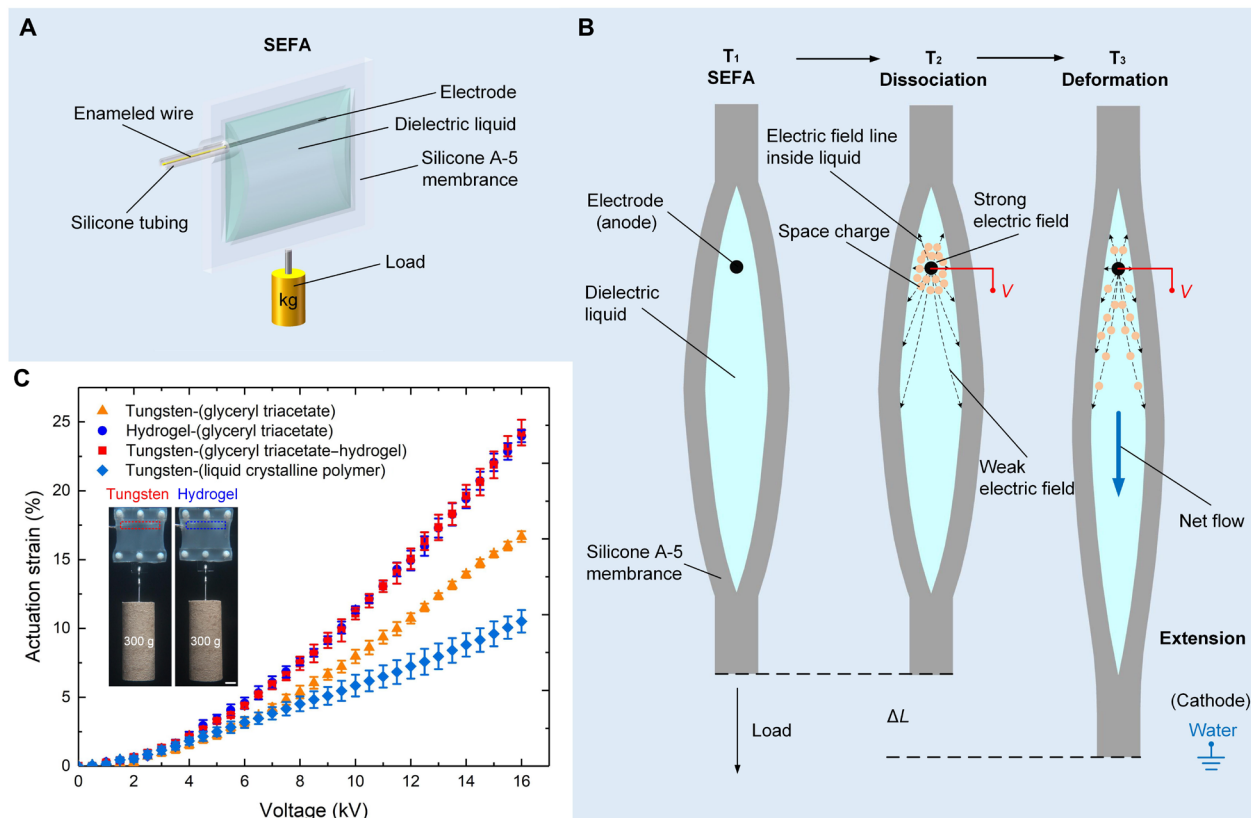


Fig. 1. Architecture, materials, and actuation mechanism of linear SEFA. (A) Architecture of linear SEFA with a load. (B) Actuation mechanism of linear SEFA. The main components of SEFA (T₁). Space charges are generated when a high voltage is applied and the surrounding water is used as electric ground (T₂). The space charges move along the electric field lines, causing ECF jet to drive the actuator extension (T₃). (C) Comparison of the actuation strain-voltage curves for four linear SEFAs. Linear SEFAs withstand a 300-g load. Scale bar, 1 cm. Photo credit: Wei Tang, Zhejiang University.

the vacuum permittivity and the relative permittivity of the liquid, respectively, and γ is the Onsager constant). Thus, it is obvious from this equation $q = -KE \cdot \nabla E$ that space charge density is determined by electric field E and its gradient ∇E . In our SEFA, electric field E gradually decreases with the electric field line from the rod positive electrode to spindle grounding electrodes. In addition, the density of the electric field line is getting smaller and smaller, that is, $\nabla E < 0$. Thus, in our actuator, the space charges are positive charges ($q = -KE \cdot \nabla E > 0$), and most of space charges will be created near the rod positive electrode because of the highest electric field E and highest ∇E . Under the Coulomb force ($F = Eq = -K(E \cdot \nabla E)E$), the space charges will migrate from the rod positive electrode along the electric field line. During this process, the migration of space charges will drag the dielectric liquid flow (31–35, 38–40), that is, ECF jet. The ECF jet will generate the actuation force. When the space charges move to the weak electric field region, the space charges will disappear because the Wien effect becomes very weak and even disappears. As long as an external electric field exists, this process will continue to occur all the time, resulting in the continuous ECF jet phenomenon shown in movie S1. Because our actuators are closed, the liquid of the jet will flow back. Continuous ECF jet and backflow occur to keep the actuator in the actuation state (elongation). When the external electric field disappears, the ECF jet disappears and the actuator goes back to the original position. Moreover, there exists a certain electrostatic extrusion effect of elastomer membrane that is caused by the voltage difference between the two sides of the elastomer membrane (see fig. S3 and table S1), and the electrostatic extrusion effect contributes a little to actuator deformation. In movie S3 and fig. S4, we have compared the performances of the actuator in its working and nonworking states when the outer membrane of SEFA is punctured by a needle. It is apparent that the actuator can continuously pump liquid out in the working state, while the liquid cannot flow out from the actuator in the nonworking state because of the high surface tension of the outer elastomer membrane.

We prepared three versions of linear SEFAs that shared the same geometry, but with different electrode materials and working fluids, demonstrating the versatility in material selection and the dependency of actuation performance on materials. Figure 1C shows the actuation performances of SEFAs made of different electrode materials (tungsten or hydrogel) and different working fluids (glyceryl triacetate or liquid crystalline polymer or glyceryl triacetate–hydrogel solution). The actuation performance of glyceryl triacetate is better than that of liquid crystalline polymer. When the dielectric liquid is glyceryl triacetate, the actuation performance of a SEFA with a hydrogel electrode is better than that of a SEFA with a tungsten electrode because a small amount of hydrogel electrode is ionized under high voltage to heighten the Wien effect so as to enhance the ECF jet behavior (movie S2). In light of this discovery, we propose a method where the hydrogel is predissociated into glyceryl triacetate to form glyceryl triacetate–hydrogel solution (fig. S5). As expected, when this glyceryl triacetate–hydrogel solution is used as dielectric liquid, the actuation performance of the SEFA with the tungsten electrode can be improved to be comparable to that of the SEFA with the hydrogel electrode (Fig. 1C and movie S1). For simplification, the easily processed tungsten electrodes were chosen in the subsequent studies. The change of the inserted rod electrode length has an obvious influence on the fluid flow and actuator performance; see movie S1 and the Supplementary Materials for details.

The actuation performance of linear SEFA increases with the applied voltage (Fig. 1C), which can achieve ~24% linear strain at 16 kV under a load of 300 g. We replaced the dielectric liquid in the pouch with an equal volume of water to turn the actuator into a type of DE actuator with the same architecture because the water inside pouch could be used as the positive electrode according to the work of Christianson *et al.* (41). Figure 2A shows the actuation performance comparison of SEFA and this type of DE actuator, where SEFA has a bit larger strains than the DE actuator under the same applied voltage. SEFA works robustly without dielectric breakdown as the voltage increases zero up to 16 kV, while the dielectric breakdown of the DE actuator occurs at 14 kV. We pierced the membrane shell of both SEFAs with a needle in their working state (fig. S4 and movie S3). After the membrane shell was punctured, the SEFA maintained its functionality to pump the liquid out without dielectric breakdown, which indicates that SEFA is safe and reliable. The effect of load on actuation strain is shown in Fig. 2B, where the actuation performance of SEFA can be improved as the load increases from zero to 250 g initially and then tends to be stable as the load further increases. The initial increase in actuation strain is due to the fact that the increase in load causes the compression in thickness to reduce the distance between the positive and ground electrodes, thereby increasing electric field intensity in the SEFA and enhancing the ECF jet effect. After the load reaches 250 g, the actuation strain tends to be stable because the further increase of the load has a slight influence on the electric field intensity.

As shown in Fig. 2C, the response time (peak time) of linear SEFA is $\sim 60 \pm 2$ ms in water and $\sim 52 \pm 2$ ms in air under a load of 300 g (which is approximately consistent with the fluid flow velocity in the linear SEFA; see the Supplementary Materials in detail), respectively. In contrast to the response speed of a traditional fluidic actuator, the highly compact SEFA that integrates the ECF jet pump, the channel, the liquid reservoir, and the actuator in a small volume between the electrodes exhibits faster response speed. Meanwhile, the SEFA with a load forms a mass-spring system, which can resonate once the excitation frequency is close to the natural frequency of the whole system. The linear SEFA achieves ~36.6% strain under a load of 350 g with a resonant frequency of 7 Hz in air (fig. S6 and movie S4). The linear SEFA has the peak strain rate of $711 \pm 66\% \text{ s}^{-1}$, the peak power density of $177 \pm 12 \text{ W kg}^{-1}$, and the work density of $7.80 \pm 0.39 \text{ J kg}^{-1}$ during contraction (fig. S8). The energy efficiency of the SEFA with glyceryl triacetate–hydrogel solution is ~9.3%. We tested the cycle life of the linear SEFA by lifting a 100-g load at an applied voltage of 14 kV and 1 Hz for 30 hours (~108,000 cycles). The test result shows that no fatigue failure and even no obvious loss in actuation are observed (fig. S9B), illustrating the durability and reliability of the actuator.

In addition, SEFAs have a key feature that allows for operational redundancy and high-force output through massive combination use. The actuation displacement can be increased by multiple SEFAs in series, while the actuation force can be amplified by multiple SEFAs in parallel. Two three-unit SEFAs in parallel can lift a heavier object to achieve a larger amplitude (Fig. 2D and movie S5). A three-unit SEFA in series is used to mimic the human antagonistic muscle stretching the joint to illustrate fast and good controllable actuation of SEFA (Fig. 2E and movie S6).

The versatility of a SEFA can be easily realized by adjusting the stiffness of the membrane shell, resembling a commonly used approach for conventional fluidic actuators (2). By replacing one of

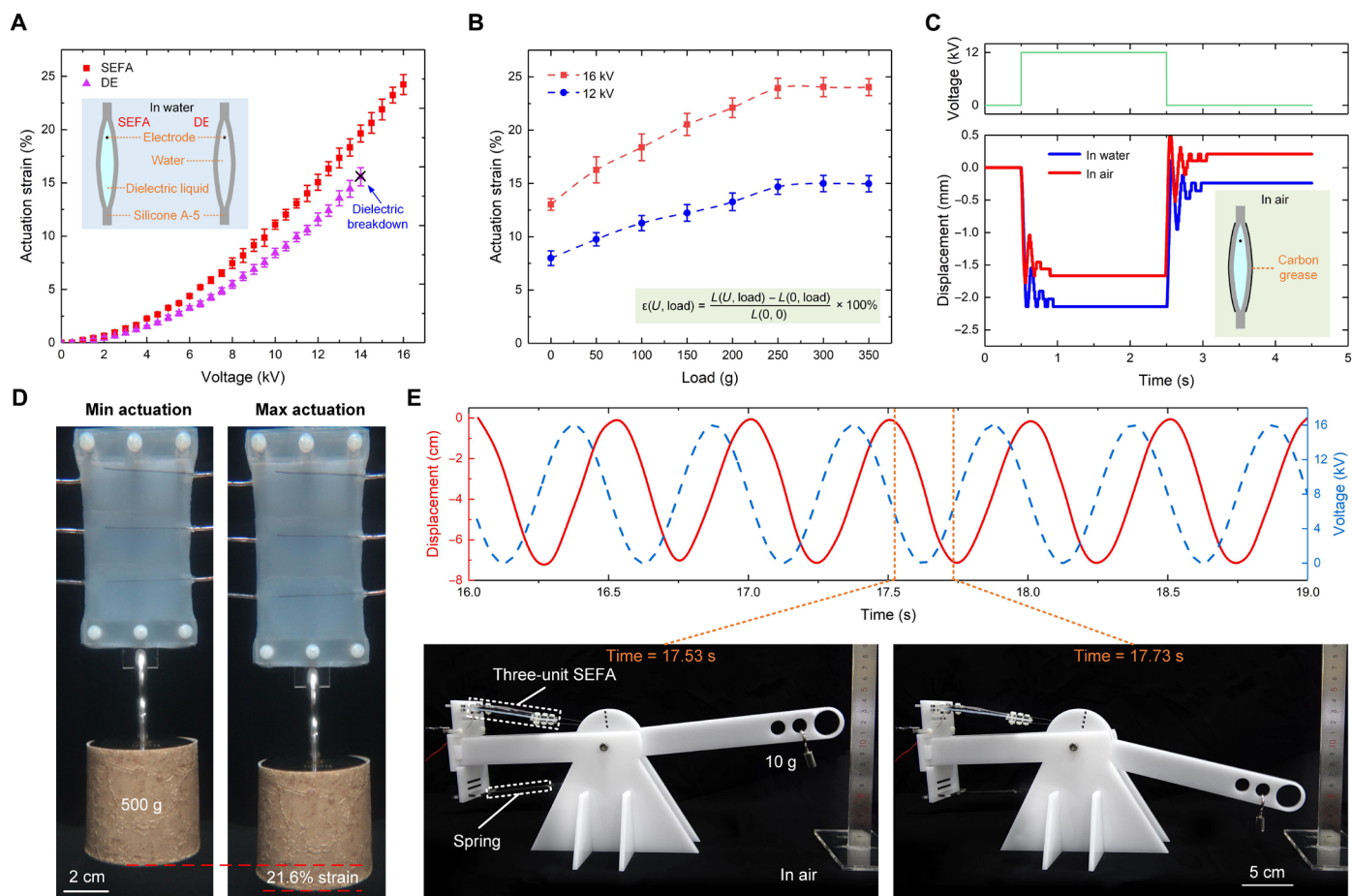


Fig. 2. Performance of linear SEFA with actuation. (A) Comparison of the actuation strain-voltage curves for DE actuator and SEFA with the same geometry and volume but different working fluids (water for DE actuator while glyceryl triacetate-hydrogel solution for SEFA) under 300-g loading. (B) Actuation strain-load curves for linear SEFAs at 12 and 16 kV. (C) Response times of SEFAs with a 300-g load in air and water are measured when 12-kV step signals are applied. Small underdamped oscillations are observed after initial extending. There is a slight difference between in air and in water because of different resistance forces of air and water and the influence of the carbon grease coated on the surface of SEFA to act as the ground electrode in air. (D) Two three-unit SEFAs in parallel with a 500-g load in water are driven by a square signal. The amplitude of the voltage is 16 kV, and the frequency is 4 Hz. (E) A three-unit SEFA in series in air is used to mimic the human antagonistic muscle stretching the joint with the help of a spring. A 10-g load is hung from the acrylic joint arm to adjust the weight of the joint arm. The SEFA is driven by a sine signal with the amplitude of 16 kV and the frequency of 2 Hz. Photo credit: Wei Tang, Zhejiang University.

the silicone A-5 membranes with a harder polydimethylsiloxane (PDMS) BD-KYN membrane, SEFA can achieve bending actuation mode due to the different deformation capabilities of silicone A-5 and PDMS BD-KYN membranes under the same force (Fig. 3A and fig. S2). We measured the bending angle, which is defined as the angle difference between the rest state without applying a voltage and the actuated state with applying the voltage, to evaluate the bending performance of the bending SEFA. The bending angle and the speed are determined by the amplitude and frequency of the applied voltage, respectively. As shown in Fig. 3B, the bending angle increases with the applied voltage, which can achieve $\sim 35.2^\circ$ at 16 kV. The bending SEFA also has a high response speed of $\sim 197 \pm 5$ ms (peak time) in water (Fig. 3C), thereby guaranteeing its agility. The response time of the bending SEFA in water is a little larger than that of the linear SEFA because the water has a greater resistance to bending motion than linear motion. The flapping speed of the bending SEFA can be adjusted by the frequency of the applied voltage. The flapping amplitude (bending angle) maintains $\sim 35.2^\circ$ when the

frequency is below 3 Hz. After the frequency exceeds 3 Hz, the flapping amplitude gradually decreases as the frequency increases (movie S7). When the frequency increases up to 30 Hz that exceeds the values of ~ 24 Hz identified by the naked eye, we can no longer identify each flapping process and thus only see a continued flapping process. Continuous operation for 30 hours at a voltage of 14 kV and 1 Hz was also conducted to test the cycle life of the bending SEFA, and the test result shows that the actuator can also keep its functionality all the time (fig. S9C).

Underwater soft robots (7, 30, 41–42) have great potential in ocean exploration; thus, we designed and fabricated a soft bionic ray with two bending SEFAs as its two fins and a flexible shell as its body (Fig. 4, A and B). A self-designed high-voltage power converter (HVPC) (fig. S10C) was encapsulated in the body of the ray to convert the low-voltage input into the high-voltage output, driving the SEFAs to advance the soft bionic ray at a low-power supply. Here, we also prepared two different untethered powering ways: battery on-board (movie S8) and wireless power transfer system

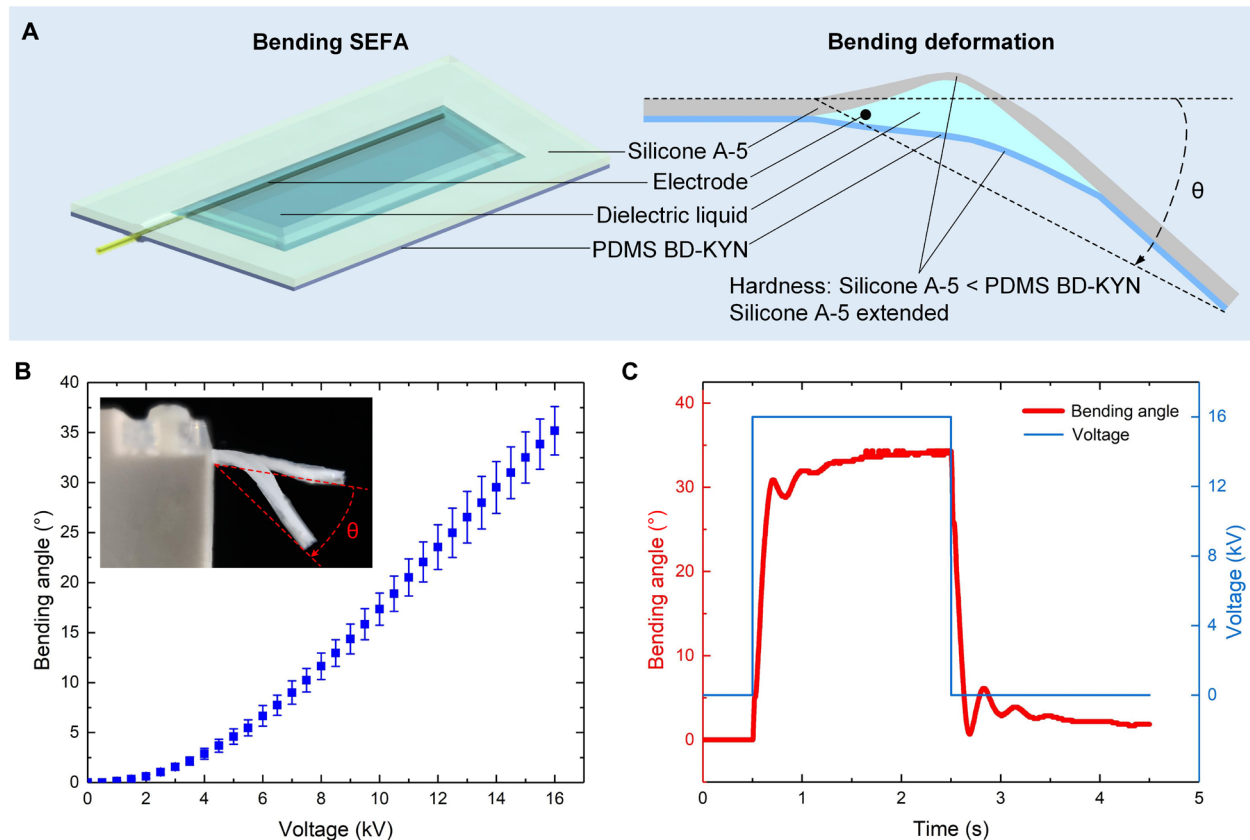


Fig. 3. Structure and performance of bending SEFA. (A) Schematic of a bending SEFA made of one silicone A-5 membrane and one PDMS BD-KYN membrane. The hardness of the PDMS BD-KYN membrane is larger than that of the silicone A-5 membrane. (B) Bending angle–voltage curves for bending SEFA. The edge of the actuator is fixed in a rigid platform, and the bending angle θ is defined as the angle difference between the original angle in the rest state and the angle in the actuated state. (C) Response time of bending SEFA in water when 16-kV step signals are applied. Photo credit: Wei Tang, Zhejiang University.

(movie S9). Figure 4C shows the scene of the soft bionic ray powered by the battery, and its swimming speed is ~ 0.13 body length per second. Figure 4D shows the architecture of a two-output AC HVPC. Compared with the battery on-board, the wireless power transfer could be an effective way to activate miniaturized robots in the future, e.g., implantable medical devices (43). Figures S11 (C and D) and S12 show the scene of the soft bionic ray powered by the wireless power transfer system. It is also worth noting that (fig. S11E) two independent high-voltage outputs in the HVPC (19) can be controlled by a mobile phone through the integrated Wi-Fi module, thereby realizing the independent remote control of two SEFAs to achieve multiple motion modes of a soft bionic ray, including swimming, turning, and spinning (fig. S11D and movie S9).

DISCUSSION

Here, we have explored a class of self-contained SEFAs, which are only manufactured by using basic fabrication techniques and widely available materials but exhibit excellent performances in safety, reliability, controllability, durability, versatility, rapid response, and excellent actuation. Meanwhile, the improvement method of dielectric liquid is proposed to enhance ECF jet in a closed elastomer, thereby improving the actuation performance of SEFAs. In addition, we have also developed HVPCs to power and control the SEFAs, offering a platform for research and development of the SEFAs as well as

other electrostatic actuators. Artificial muscle stretching a joint, a compliant gripper catching a live goldfish, and a soft bionic ray swimming in a tank illustrate the wide potential of SEFAs for next-generation soft robotics.

Relative to existing fluidic actuators (10, 15–19, 27–29), including soft fluidic actuators driven by separated ECF jet pumps or traditional rigid pumps, SEFAs that highly integrate pumps, tubes, liquid reservoirs, and actuators not only exhibit better portability but also show excellent response to electrical signals. Several detailed actuation performances of the SEFAs and some existing soft actuators, including strain rate, power, and energy density, are indicated in table S2. SEFAs are expected to consume more electrical power than DE actuators and HASEL actuators because of the viscous loss of fluid flow. Actuation performance of SEFAs could be further improved by adjusting the hardness and thickness of the elastomer membrane or the characteristics of the dielectric liquid. Overall, SEFAs strike a balance among several indispensable properties for human-robot interaction devices, including safety, controllability, rapid response, and excellent actuation.

Although SEFAs present several promising features, there remain some challenges to resolve current limitations of SEFAs. An existing hurdle is that the dielectric liquid driven by high voltage is used in the current SEFAs, and future studies need to reduce the operating voltage through the use of alternate fluids that could be driven by low voltage or alternate materials of pouch. Meanwhile,

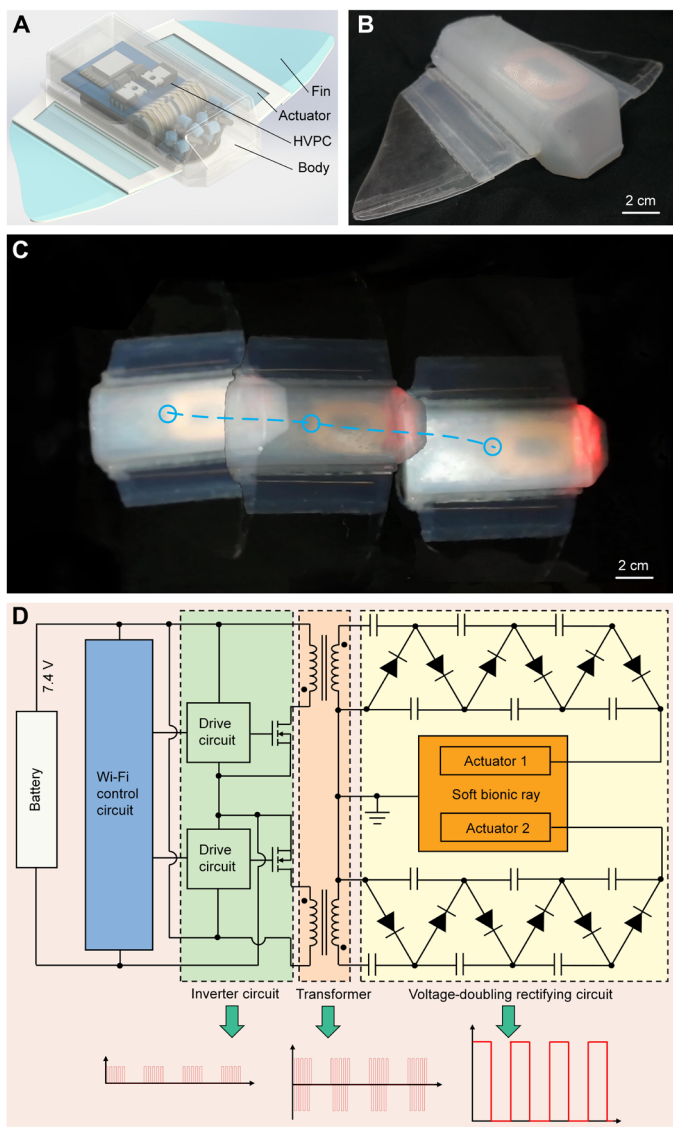


Fig. 4. Soft bionic ray actuated by two bending SEFAs. (A) Computer-generated rendering of the soft bionic ray. (B) Photograph of the actual soft bionic ray. (C) Time lapse of the swimming motions of the soft bionic ray. (D) Architecture of two-output AC HVPC powered by battery. The circuit consists of three parts: an inverter circuit that converts 7.4-V DC to an intermittent high-frequency square wave pulse, a high-frequency transformer that boosts the AC voltage, and a voltage-doubling rectifying circuit that rectifies the high-frequency AC into intermittent DC (square wave). Photo credit: Wei Tang, Zhejiang University.

there is a potential risk that the high-voltage electrode will be attracted to contact the solid pouch so as to cause the dielectric breakdown of the pouch if the actuator is strained too much. Therefore, it is better to find some effective methods to protect the membranes that are close to the positive electrode. Tungsten electrodes and hydrogel electrodes are used in this work. The problems of physical piercing and the mismatch between tungsten electrodes and soft surrounding membranes exist, while these problems could be addressed by the use of hydrogel electrodes. Therefore, other suitable soft conductive materials, such as conductive silicone, could also be

used to avoid these problems. In addition, SEFAs consume more electrical power than other electrostatic actuators such as DE actuators or HASEL actuators because of energy loss of fluid flow.

In this study, the electrically responsive fluids in a closed elastomer are used to develop SEFAs, but other ways of stimuli-responsive fluids, such as magnetically responsive fluids and photo-responsive fluids, might also be explored to achieve this target. Although the preliminary exploration of the wireless power transfer technology is conducted to power the SEFA, a one-to-many and long-distance all-round wireless power supply method should be explored in the future.

MATERIALS AND METHODS

Actuator materials

SEFAs consisted of three basic components: flexible pouch, electrode, and dielectric liquid. The flexible pouch of SEFA was made of silicone A-5 membranes (PS6650-5du and translucency, China Shenzhen Yipin Trading Co. Ltd.), a PDMS BD-KYN membrane (BD Film KYN-300, China Hangzhou Bald Advanced Materials Co. Ltd.), or both of them. Three sets of uniaxial tensile tests were conducted at an ASTM D638 (Type IV) universal test machine with a crosshead speed of 50 mm/min (19) to evaluate deformation capacities of the silicone A-5 and PDMS BD-KYN membranes (fig. S2). The tap water was used as electrodes, of which the conductivity was $\sim 2 \times 10^{-2}$ S/m. Three kinds of dielectric liquid, including glyceryl triacetate (G103099, Aladdin), glyceryl triacetate-hydrogel solution, and liquid crystalline polymer, were used for SEFAs. The conductivity and permittivity of glyceryl triacetate were $\sim 1.13 \times 10^{-8}$ S/m (liquid conductivity meter) and 5.0867 (vector network analyzer, coaxial reflection method, measurement frequency is 1 GHz), respectively. The conductivity and permittivity of glyceryl triacetate-hydrogel solution were $\sim 1.45 \times 10^{-8}$ S/m and 5.4646, respectively. The pouch was fabricated by bonding two flexible membranes using an adhesive method. More details of SEFA materials, fabrication, and testing methods can be found in the Supplementary Materials.

Demonstration of artificial muscle stretching joint

To demonstrate rapid, good controllable actuation of SEFA, a three-unit SEFA in series and a spring were assembled and attached to an acrylic joint, resembling the motion mechanism of antagonistic muscles such as biceps and triceps. A 10-g load was hung from the joint arm for adjusting the weight of the joint arm, and the end of the joint arm was used as the output instead of movement angle for ease of measurement. Sine waves with different amplitudes were applied to test the joint, and the demonstration of actuation is shown in Fig. 2E and movie S6.

High-voltage power converter

We designed and fabricated two HVPCs: a DC HVPC and an AC HVPC. The DC HVPC adopted a conventional topology that consisted of a pulse oscillating circuit, an inverter circuit, a high-frequency transformer, and a voltage-doubling rectifying circuit (fig. S10A) (19, 44–45). Two AC outputs were realized by a Wi-Fi module connecting with two DC HVPCs (19) and realized two independent outputs through the control of a mobile phone. A high-voltage probe (P6015, Trek) and an oscilloscope (InfiniiVision 2000 X-Series, Keysight) were used to test the output of the HVPCs (19), and the results are shown in fig. S10 (D to I).

Wireless power transfer system

The wireless power transfer (19, 46–47) system was mainly composed of 50 emitting circuit modules, 50 emitting coils, 2 receiving circuit modules, 2 receiving coils, a nonmagnetic shim, 50 relays, a power supply, a microcontroller, and a two-layer nylon plate frame (fig. S12 and movie S9).

Fabrication of a soft bionic ray

Two bending SEFAs were used to actuate a soft bionic ray. An L-shaped 1-mm-thick acrylic board was glued in the edge of the fins. The body of the soft bionic ray was three-dimensionally printed using thermoplastic elastomer (TPE). A two-output AC HVPC, two receiving circuit modules, and two receiving coils were embedded in the ray's body, and a wire was installed as its tail. The ray's body was sealed using acrylic glue. The two SEFAs of the soft bionic ray were independently controlled by a mobile phone, achieving different motions such as swimming, turning, and spinning (fig. S11D and movie S9).

SUPPLEMENTARY MATERIALS

Supplementary material for this article is available at <http://advances.sciencemag.org/cgi/content/full/7/34/eabf8080/DC1>

REFERENCES AND NOTES

- M. Cianchetti, C. Laschi, A. Menciassi, D. Paolo, Biomedical applications of soft robotics. *Nat. Rev. Mater.* **3**, 143–153 (2018).
- D. Rus, M. T. Tolley, Design, fabrication and control of soft robots. *Nature* **521**, 467–475 (2015).
- Y. Kim, G. A. Parada, S. Liu, X. Zhao, Ferromagnetic soft continuum robots. *Sci. Robot.* **4**, eaax7329 (2019).
- R. F. Shepherd, F. Illievski, W. Choi, S. A. Morin, A. A. Stokes, A. D. Mazzeo, X. Chen, M. Wang, G. M. Whitesides, Multigait soft robot. *Proc. Natl. Acad. Sci. U.S.A.* **108**, 20400–20403 (2011).
- G. Mao, M. Drack, M. Karami-Mosammam, D. Wirthl, T. Stockinger, R. Schwödauer, M. Kaltenbrunner, Soft electromagnetic actuators. *Sci. Adv.* **6**, eabc0251 (2020).
- Y. Tang, Y. Chi, J. Sun, T.-H. Huang, O. H. Maghsoudi, A. Spence, J. Zhao, H. Su, J. Yin, Leveraging elastic instabilities for amplified performance: Spine-inspired high-speed and high-force soft robots. *Sci. Adv.* **6**, eaaz6912 (2020).
- R. K. Katschmann, J. DelPreto, R. MacCurdy, D. Rus, Exploration of underwater life with an acoustically controlled soft robotic fish. *Sci. Robot.* **3**, eaar3449 (2018).
- N. W. Xu, J. O. Dabiri, Low-power microelectronics embedded in live jellyfish enhance propulsion. *Sci. Adv.* **6**, eaaz3194 (2020).
- L. Hines, K. Petersen, G. Z. Lum, M. Sitti, Soft actuators for small-scale robotics. *Adv. Mater.* **29**, 1603483 (2017).
- S. I. Rich, R. J. Wood, C. Majidi, Untethered soft robotics. *Nat. Electron.* **1**, 102–112 (2018).
- E. Acome, S. K. Mitchell, T. G. Morrissey, M. B. Emmett, C. Benjamin, M. King, M. Radakovic, C. Keplinger, Hydraulically amplified self-healing electrostatic actuators with muscle-like performance. *Science* **359**, 61–65 (2018).
- N. Kellaris, V. Gopaluni Venkata, G. M. Smith, S. K. Mitchell, C. Keplinger, Peano-HASEL actuators: Muscle-mimetic, electrohydraulic transducers that linearly contract on activation. *Sci. Robot.* **3**, eaar3276 (2018).
- H. Lu, M. Zhang, Y. Yang, Q. Huang, T. Fukuda, Z. Wang, Y. Shen, A bioinspired multilegged soft millirobot that functions in both dry and wet conditions. *Nat. Commun.* **9**, 3944 (2018).
- X. Wang, C. Ho, Y. Tsatskis, J. Law, Z. Zhang, M. Zhu, C. Dai, F. Wang, M. Tan, S. Hopyan, H. McNeill, Y. Sun, Intracellular manipulation and measurement with multipole magnetic tweezers. *Sci. Robot.* **4**, eaav6180 (2019).
- P. Polygerinos, N. Correll, S. A. Morin, B. Mosadegh, C. D. Onal, K. Petersen, M. Cianchetti, M. T. Tolley, R. F. Shepherd, Soft robotics: Review of fluid-driven intrinsically soft devices; manufacturing, sensing, control, and applications in human-robot interaction. *Adv. Eng. Mater.* **19**, 1700016 (2017).
- V. Cacciuolo, J. Shintake, Y. Kuwajima, S. Maeda, D. Floreano, H. Shea, Stretchable pumps for soft machines. *Nature* **572**, 516–519 (2019).
- M. A. Meller, M. Bryant, E. Garcia, Reconsidering the McKibben muscle: Energetics, operating fluid, and bladder material. *J. Intell. Mater. Syst. Struct.* **25**, 2276–2293 (2014).
- M. Wehner, M. T. Tolley, Y. Mengüç, Y.-L. Park, A. Mozeika, Y. Ding, C. Onal, R. F. Shepherd, G. M. Whitesides, R. J. Wood, Pneumatic energy sources for autonomous and wearable soft robotics. *Soft Robot.* **1**, 263–274 (2014).
- W. Tang, C. Zhang, Y. Zhong, P. Zhu, Y. Hu, Z. Jiao, X. Wei, G. Lu, J. Wang, Y. Liang, Y. Lin, W. Wang, H. Yang, J. Zou, Customizing a self-healing soft pump for robot. *Nat. Commun.* **12**, 2247 (2021).
- X. Huang, K. Kumar, M. K. Jawed, A. M. Nasab, Z. Ye, W. Shan, C. Majidi, Chasing biomimetic locomotion speeds: Creating untethered soft robots with shape memory alloy actuators. *Sci. Robot.* **3**, eaau7557 (2018).
- J. M. Jani, M. Leary, A. Subic, M. A. Gibson, A review of shape memory alloy research, applications and opportunities. *Mater. Des.* **56**, 1078–1113 (2014).
- R. Pelrine, R. Kornbluh, Q. Pei, J. Joseph, High-speed electrically actuated elastomers with strain greater than 100%. *Science* **287**, 836–839 (2000).
- F. Carpi, S. Bauer, D. De Rossi, Stretching dielectric elastomer performance. *Science* **330**, 1759–1761 (2010).
- Y. Qiu, E. Zhang, R. Plamthottam, Q. Pei, Dielectric elastomer artificial muscle: Materials innovations and device explorations. *Acc. Chem. Res.* **52**, 316–325 (2019).
- P. Brochu, Q. Pei, Advances in dielectric elastomers for actuators and artificial muscles. *Macromol. Rapid Commun.* **31**, 10–36 (2010).
- S. Diahm, S. Zelmat, M.-L. Locatelli, S. Dinculescu, M. Decup, T. Lebey, Dielectric breakdown of polyimide films: Area, thickness and temperature dependence. *IEEE Trans. Dielectr. Electr. Insul.* **17**, 18–27 (2010).
- A. Yamaguchi, K. Takemura, S. Yokota, K. Edamura, A robot hand using electro-conjugate fluid: Grasping experiment with balloon actuators inducing a palm motion of robot hand. *Sens. Actuat. A Phys.* **174**, 181–188 (2012).
- S. Ueno, K. Takemura, S. Yokota, K. Edamura, Micro inchworm robot using electro-conjugate fluid. *Sens. Actuat. A Phys.* **216**, 36–42 (2014).
- K. Takemura, S. Yokota, K. Edamura, Development and control of a micro artificial muscle cell using electro-conjugate fluid. *Sens. Actuat. A Phys.* **133**, 493–499 (2007).
- T. Li, G. Li, Y. Liang, T. Cheng, J. Dai, X. Yang, B. Liu, Z. Zeng, Z. Huang, Y. Luo, T. Xie, W. Yang, Fast-moving soft electronic fish. *Sci. Adv.* **3**, e1602045 (2017).
- D. S. Cho, S. Kang, Y. K. Suh, Development of a bi-directional electrohydrodynamic pump: Parametric study with numerical simulation and flow visualization. *Adv. Mech. Eng.* **8**, 1–15 (2016).
- D. V. Fernandes, Y. K. Suh, Numerical simulation and design optimization of an electrohydrodynamic pump for dielectric liquids. *Int. J. Heat Fluid Fl.* **57**, 1–10 (2016).
- D. V. Fernandes, D. S. Cho, Y. K. Suh, Electrohydrodynamic flow of dielectric liquid around a wire electrode – effect of truncation of onsager function. *IEEE Trans. Dielectr. Electr. Insul.* **21**, 194–200 (2014).
- J.-w. Kim, Y. Tanabe, S. Yokota, Comprehending electro-conjugate fluid (ECF) jets by using the Onsager effect. *Sens. Actuat. A Phys.* **295**, 266–273 (2019).
- Y. K. Suh, Modeling and simulation of ion transport in dielectric liquids – Fundamentals and review. *IEEE Trans. Dielectr. Electr. Insul.* **19**, 831–848 (2012).
- L. Onsager, Deviations from Ohm's law in weak electrolytes. *J. Chem. Phys.* **2**, 599–615 (1934).
- J. C. Ryu, H. J. Park, J. K. Park, K. H. Kang, New electrohydrodynamic flow caused by the Onsager effect. *Phys. Rev. Lett.* **104**, 104502 (2010).
- S. A. Vasilkov, V. A. Chirkov, Y. K. Stishkov, Electrohydrodynamic flow caused by field-enhanced dissociation solely. *Phys. Fluids* **29**, 063601 (2017).
- R. V. Raghavan, J. Qin, L. Y. Yeo, J. R. Friend, K. Takemura, S. Yokota, K. Edamura, Electrokinetic actuation of low conductivity dielectric liquids. *Sens. Actuat. B Chem.* **140**, 287–294 (2009).
- M. A. W. Siddiqui, J. Seyed-Yagoobi, Experimental study of pumping of liquid film with electric conduction phenomenon. *IEEE Trans. Indust. Appl.* **45**, 3–9 (2009).
- C. Christianson, N. N. Goldberg, D. D. Deheyne, S. Cai, M. T. Tolley, Translucent soft robots driven by frameless fluid electrode dielectric elastomer actuators. *Sci. Robot.* **3**, eaat1893 (2018).
- W.-S. Chu, K.-T. Lee, S.-H. Song, M.-W. Han, J.-Y. Lee, H.-S. Kim, M.-S. Kim, Y.-J. Park, K.-J. Cho, S.-H. Ahn, Review of biomimetic underwater robots using smart actuators. *Int. J. Precis. Eng. Manuf.* **13**, 1281–1292 (2012).
- R. V. Taalla, M. S. Arefin, A. Kaynak, A. Z. Kouzani, A review on miniaturized ultrasonic wireless power transfer to implantable medical devices. *IEEE Access* **7**, 2092–2106 (2019).
- J.-W. Yang, H.-L. Do, Soft-switching dual-flyback DC–DC converter with improved efficiency and reduced output ripple current. *IEEE Trans. Indust. Electron.* **64**, 3587–3594 (2017).
- W.-C. Hsu, J.-F. Chen, Y.-P. Hsieh, Y.-M. Wu, Design and steady-state analysis of parallel resonant DC–DC converter for high-voltage power generator. *IEEE Trans. Power Electron.* **32**, 957–966 (2017).
- Z. Zhang, H. Pang, A. Georgiadis, C. Cecati, Wireless power transfer—An overview. *IEEE Trans. Indust. Electron.* **66**, 1044–1058 (2018).
- H. De Clercq, R. Puers, Contactless energy transfer at the bedside featuring an online power optimization strategy. *Sens. Actuat. A Phys.* **217**, 160–167 (2014).
- H. Yuk, T. Zhang, S. Lin, G. A. Parada, X. Zhao, Tough bonding of hydrogels to diverse non-porous surfaces. *Nat. Mater.* **15**, 190–196 (2016).

49. D. Yang, M. S. Verma, J.-H. So, B. Mosadegh, C. Keplinger, B. Lee, F. Khashai, E. Lossner, Z. Suo, G. M. Whitesides, Buckling pneumatic linear actuators inspired by muscle. *Adv. Mater. Technol.* **1**, 1600055 (2016).
50. J. D. W. Madden, N. A. Vandesteeg, P. A. Anquetil, P. G. A. Madden, A. Takshi, R. Z. Pytel, S. R. Lafontaine, P. A. Wieringa, I. W. Hunter, Artificial muscle technology: Physical principles and naval prospects. *IEEE J. Oceanic Eng.* **29**, 706–728 (2004).

Acknowledgments: We thank S. Tang, Z. Du, and P. Zhu for help with circuit designing, video shooting, picture processing, and experiment designing. **Funding:** This work is supported by the National Natural Science Foundation of China (award nos. 51875507 and 51890885) and the Fundamental Research Funds for the Central Universities (no. 2020QNA4003). **Author contributions:** W.T., C.Z., J.Z., and H.Y. conceived the idea and designed the research. W.T., Y.Lin, C.Z., Y.Lia., J.W., W.W., C.J., and M.Z. conducted the experimental work. W.T. developed

the HVPC and the wireless power transfer system. W.T., C.Z., and J.Z. analyzed the data. W.T., C.Z., and J.Z. wrote the manuscript with input from all authors. **Competing interests:** The authors declare that they have no competing interests. **Data and materials availability:** All data needed to evaluate the conclusions in the paper are present in the paper and/or the Supplementary Materials.

Submitted 20 November 2020

Accepted 30 June 2021

Published 20 August 2021

10.1126/sciadv.abf8080

Citation: W. Tang, Y. Lin, C. Zhang, Y. Liang, J. Wang, W. Wang, C. Ji, M. Zhou, H. Yang, J. Zou, Self-contained soft electrofluidic actuators. *Sci. Adv.* **7**, eabf8080 (2021).